Earth **Surface**
Dynamics
Discussions

Detection of seasonal erosion processes at the scale of an elementary black marl gully from time series of Hi-Resolution DEMs

J. Bechet[1,†], J. Duc[1], A. Loye[1], M. Jaboyedoff[1], N. Mathys[2], J.-P. Malet[3],
S. Klotz[2], C. Le Bouteiller[2], B. Rudaz[1], and J. Travelletti[3,a]

[1]University of Lausanne, Risk-group – ISTE – Institute of Earth Sciences,
Lausanne, Switzerland
[2]IRSTEA Grenoble, Unité de recherche Erosion Torrentielle, Neige et Avalanches, BP 76,
38402 Saint Martin d'Hères, France
[3]Institut de Physique du Globe de Strasbourg, CNRS UMR 7516, Ecole et Observatoire des
Sciences de la Terre, Université de Strasbourg, 5 rue Descartes, 67084 Strasbourg, France
[a]now at: BEG – Bureau d'Etudes Géologiques SA, Rue de la Printse 4,
1994 Aproz, Switzerland
[†]deceased, 28 March 2015

Title Page

Abstract | Introduction

Conclusions | References

Tables | Figures

◄ | ►

◄ | ►

Back | Close

Full Screen / Esc

Printer-friendly Version

Interactive Discussion

Detection of seasonal erosion processes at the scale of an elementary black marl gully

J. Bechet et al.

Full Screen / Esc

Printer-friendly Version

Interactive Discussion

Detection of seasonal erosion processes at the scale of an elementary black marl gully

J. Bechet et al.

Abstract

The Roubine catchment located in the experimental research station of Draix-Bléone (south French Alps) is situated in Callovo-Oxfordian black marls, a lithology particularly prone to weathering processes. Since 30 years, this small watershed (0.13 ha) has been monitored for analysing hillslope erosion processes at the scale of elementary gullies.

Since 2007, a monitoring of surface changes has been performed by comparing of high-resolution digital elevation models (HR-DEMs) produced from Terrestrial Laser Scanner (TLS). The objectives are (1) to detect and (2) to quantify the sediment production and the evolution of the gully morphology in terms of sediment availability/transport capacity vs. rainfall and runoff generation. Time series of TLS observations have been acquired periodically based on the seasonal runoff activity with a very high point cloud density ensuring a resolution of the DEM at the centimetre scale. The topographic changes over a time span of 4 years are analysed.

Quantitative analyses of the seasonal erosion activity and of the sediment fluxes contributing to the recharge of tributary gullies and rills are presented. According to the transport capacity generated by runoff, loose regolith soil sources are eroded at different periods of the year. These are forming transient deposits in the main reach when routed downstream, evolving from a transport-limited to a supply-limited regime through the year. The monitoring allows a better understanding of the seasonal pattern of erosion processes for black marls badland-type slopes and illustrates the mode of sediment production and the temporal storage/entrainment in similar slopes. The observed surface changes caused by erosion (ablation/deposition) are quantified for the complete TLS time-series, and sediment budget maps are presented for each season. Comparisons of the TLS sediment budget map with the in situ sediment monitoring (limnigraph and sedigraph) in the stream are discussed. Intense and long duration rainfall events are the triggering factor of the major erosive events.

1 Introduction

Jurassic black marls of Callovo-Oxfordian age (e.g. also called "*Terres Noires*") cover large areas in South-East France. The badland landscape observed in these clay-shales catchments is the result of the conjunction of favorable lithological and climatic factors. Freeze–thaw and wetting–drying cycles progressively disintegrate the black marls formation thus favoring the annual development of a weathered marly layer exposed to surface runoff erosion and shallow landslides (Antoine et al., 1995; Maquaire et al., 2003). The weathered marls can be mobilized by Hortonian runoff especially during high-intensity rainfalls in summer. This causes flash floods and hyperconcentrated flows inducing significant problems in sedimentation reservoirs and river systems (Oostwoud Wijdenes and Ergenzinger, 1998; Descroix and Olivry, 2002). Saturation of the weathered marls layers can also locally trigger shallow landslides supplying high sediment loads to the basins. In addition, rain infiltration in the fractured marls bedrock contributes to the triggering of larger landslides whose geometry is controlled by the bedding and the discontinuities. There is a strong seasonal difference between the rates of surface erosion processes in summer and winter (Descroix and Gautier, 2002; Descroix and Mathys, 2003); the erosion processes have therefore an annually-cyclic activity pattern.

Among the cross-disciplinary research activities conducted in the Draix-Bléone catchments (SOERE RBV), composed of seven nested catchments characterized by several sizes and vegetation cover, this work focuses on the analysis of the processes controlling the annual pattern of erosion rates in elementary gullies (Richard, 1997; Meunier and Mathys, 1995; Mathys et al., 2005).

Terrestrial Laser Scanner (TLS) is a powerful tool to monitor erosion processes at the gully scale at a relatively low cost (Perroy et al., 2010; Jaboyedoff et al., 2012) where high spatial resolution data on surface changes is needed (Jacome, 2009). Such high resolution mapping of erosion rates at fine (e.g. seasonal) temporal scale for an entire catchment is innovative and represents considerable progress in the field of erosion

Title Page

Abstract | Introduction

Conclusions | References

Tables | Figures

◄ | ►

◄ | ►

Back | Close

Full Screen / Esc

assessment (Lopez Saez et al., 2011). Preliminary studies show a great potential of TLS to measure and map surface erosion (Puech et al., 2009) since it can detect millimetric-scale changes at short range distances (50 m; Abellán et al., 2009).

In this study, time series of intra-annual TLS observations are used to quantify sur-
5   face erosion. The main objectives are: (i) to create ablation and deposition maps for every season, (ii) to estimate the sediment budget and evaluate the accuracy of the volume calculation at the catchment scale by comparing it to sediment trap observa-tion and (iii) to propose a conceptual model explaining the observed seasonal pattern of ablation and deposition. The results allow identifying and quantifying the topographic
10 changes of the catchment in terms of regolith development, slope transfer processes, and transient storages of sediment within the rills and gullies. This is put in perspective with previous work on similar black marls slopes.

2   Physio-geographic settings of the study area: the Roubine catchment

2.1   Morphology

15 The research has been conducted in the Draix-Bléone experimental catchments (SO-ERE RBV network, *Systèmes d'Observation et d'Expérimentation pour la Recherche en Environnement Réseau de Bassins Versants*) in southeast France, near the city of Digne-les-Bains (Alpes-de-Haute-Provence). Draix-Bléone observatory is composed of seven small mountain watersheds. It was created by IRSTEA in 1983 in order to bet-
20 ter understand erosion and sediment transfer processes, including hyperconcentrated floods, and to improve the design of protections in response to erosion processes. The experimental site selected for this work is the Roubine elementary catchment (Fig. 1), which is the smallest monitored (1030 m^2) watershed of the Draix experimental site (Mathys et al., 2003). No human actions have been conducted within the gully since
25 the setup of the observatory in 1983.

This elementary watershed has a typical badland morphology characterized by V-shaped gullies, steep slopes (35–45°) and a low vegetation coverage (ca. 20 %). The Roubine elementary catchment is constituted by one main gully that crosses it from East to West. This gully separates the catchment into a north- and a south-facing slope. On the south-facing slope, a secondary gully crosses diagonally in the direction North-east to South-west and confluences with the main gully at the catchment outlet. Both north and south-facing slopes are braided with many small gullies and rills of decametric widths. A few un-weathered marl outcrops can be observed in the steepest sections of both slopes. On these outcrops, the dip of the black marl formation is 30° to the East. The scarce vegetation cover is constituted of a few black pines (*Pina Negra*) and tuffs of grass restricted to the flatter interfluves near the sediment trap and on the top of the crests.

A sediment trap, a stream gauge and an automatic sampler are installed at the bottom of La Roubine in order to monitor the sediment yield and the water discharge (Mathys et al., 2003). Rainfall observations are collected by a rain gauge located 20 m from the Roubine outlet.

2.2 Geology

Large areas of Southeast France are covered by black marls which outcrop over more than $10\,000\,km^2$ in the watershed of the Durance river (Légier, 1977; Phan and Antoine, 1994; Mathys et al., 1996). This sedimentary lithology is composed of alternating marl and limestone sequences whose ages range from Lias to Cretaceous. The marly sequence which outcrops in the Draix-Bléone catchments is from the Bathonian to Oxfordian, and its thickness can exceed 2000 m in some places (Antoine et al., 1995; Maquaire et al., 2003). A limestone ridge overlies the black marls (Ballais, 1999).

2.3 Climate

Slope erosion rates are influenced by the specific features of a Mediterranean mountain climate with strong seasonal and yearly differences in temperature and rainfall. At Draix, the mean annual rainfall is 920 mm with an interannual- variability of nearly 400 mm over the period 1970–2000. The summer is relatively dry, but several heavy thunderstorms can occur, which intensity sometimes exceeds 60 mm h^{-1} (Richard, 1997) and can even reach more than 100 mm h^{-1} during a few minutes (Yamakoshi et al., 2009), i.e. 210, 138, 90, 74 and 45 mm h^{-1} respectively during 1, 5, 15, 30 and 60 min (Mathys, 2006). These events trigger hyper concentrated flows characterized by suspended sediment discharge of up to 800 g L^{-1} (Olivier, 1999). Micro-debris flows (MDFs) have also been observed (Oostwoud Wijdenes and Ergenzinger, 1998), and clearly associated with high erosive events (Yamakoshi et al., 2009, 2010). Hailstorms are not unusual. During spring and autumn seasons, the rainfall amounts are at their maxima. During the winter, very small amounts of rainfall are measured, but over 100 cycles of freezing-thawing are observed (Oostwoud Wijdenes and Ergenzinger, 1998; Rovera and Robert, 2005). A snow cover can form but does not usually last the whole winter. The daily average air temperature is 10.9 °C with a standard deviation of 8.7 °C, over the period 1970–2000.

2.4 Hillslope activity processes

The alternating of freezing-thawing and wetting-drying cycles is the key process controlling the development of a weathered loose regolith on black marl slopes (Maquaire et al., 2002; Brochot et Meunier, 1994). At the end of the winter season, a thick layer of loose regolith can accumulate in the lower parts of the slopes and at the outlets of the gullies. The south-facing slope is characterized by a higher number of weathering cycles than the north-facing slope (Maquaire et al., 2002). But considering only the freezing and thaw cycles the south-facing slope suffer more cycles than the north-facing ones, but in the gullies the south-facing slope are equivalent to north facing slope

(Rovera and Robert, 2005). However the north-facing slopes present higher depths of frozen soils. The pattern of erosion rates is therefore strongly controlled by the slope exposition and aspect. In addition, it has been demonstrated that erosion rates increase with increasing slope angle on bare marls (Lopez-Saez et al., 2001).

The slope surfaces evolve dynamically through the year. The un-weathered black marls density is $2650\,\mathrm{kg\,m^{-3}}$, while the regolith density can be as small as $1300\,\mathrm{kg\,m^{-3}}$ but it varies greatly in space and time according to the presence of local discontinuities (Maquaire et al., 2003; Travelletti et al., 2012). The measurements of the densities of the black marl deposited in the sediment trap vary from $1500\,\mathrm{kg\,m^{-3}}$ to $1800\,\mathrm{kg\,m^{-3}}$ (Mathys et al., 1996). In the spring season, the regolith observed in the gullies has a popcorn structure and therefore a low density. In the summer season, sedimentary and structural thin crusts can develop at the surface of the regolith because of the intense wetting (Malet et al., 2003). The mean erosion rate of the black marls is of $8\,\mathrm{mm\,yr^{-1}}$, which is approximately $100\,\mathrm{t\,ha^{-1}\,yr^{-1}}$ (Olivry and Hoorelbeck, 1989), and more specifically of $100\,\mathrm{t\,ha^{-1}\,yr^{-1}}$ or $13\,\mathrm{mm\,yr^{-1}}$ for La Roubine catchment. In the absence of shallow mass movements, the lower parts of the slopes are, generally, eroded by runoff at the same rate as the interfluves and the upper parts the slopes; this system yields to relatively constant slope gradient values over time (Descroix and Mathys, 2003).

3 Methodology

3.1 Terrestrial Laser Scanner (TLS) measurements

The study site has been monitored using a Terrestrial Laser Scanning system (TLS). This remote scanning device is a monochromatic laser pulse transmitter/receiver. The laser beam pulses are oriented using mirrors or by moving the laser source mechanically or both. The time of flight (TOF) is the time for the pulses to travel the double distance (d), at the light velocity (c), to the reflecting surfaces ($2 \times d = c \times \mathrm{TOF}$). In

practice the laser as a footprint that increases in diameter with increasing distances to the target. The operation is repeated millions of times giving access to a very dense grid of XYZ points (Shan and Toth, 2008). Two types of TLS were used for this study: TLS1 is an Ilris 3-D (Optech, Canada) scanner, and TLS2 is a TotalStation II (Leica, Germany) scanner. The TLS1 laser is infrared (1535 nm) and the performance coming from the manufacturer indicates that it produces data with an accuracy of 8 mm with a spot diameter of 22 mm at 100 m. The TLS2 laser is in the green electromagnetic spectrum (give wavelength) with a 6 mm accuracy and a 6 mm spot size at 50 m.

3.2   Data acquisition and processing

Twelve TLS campaigns were performed from the 9 May 2007 to the 4 November 2010 (Table 1). The data of the years 2007 and 2008 is sparser as the methodology and protocol were being developed. In 2009 and 2010, TLS data were acquired more regularly through the year in order to take into account more precisely the influences of the seasonal rainfall.

For each TLS campaign, the measures were performed from up to five different scan positions in order to minimize shadow areas. However, some shadow areas still remain because of the presence of foreground in the line of sight of the scanner or of vegetation. All scan spatial resolutions are of less than 10 mm at a 50 m distance range. The point cloud density is very high for all the time series and range among 0.3 to 3 pts cm^{-2}.

The software Polyworks V.10 (InnovMetric, 2010) has been used to process the TLS point clouds. First, the vegetated areas are deleted from the raw point clouds in order to keep for the analysis only the bare soil surface. The scans of each campaign are then aligned using the Iterative Closest Point (ICP) procedure (Chen and Medioni, 1992; Besl and McKay, 1992) to obtain a point cloud of the entire catchment. The TLS campaigns are aligned to a reference campaign (e.g. June 2009) using eight white 180 mm diameter styrene-spheres located around the catchment since 2008. Depending on the TLS distance of acquisition and the overlapping of the different scenes, the

final point cloud density is variable; thus, each TLS point cloud has been interpolated using Surfer (GoldenSoftware 8) inverse distance method (Shepard, 1968) into a homogeneous high resolution (0.02 m) High Resolution Digital Elevation Model (HRDEM). A high density point cloud produces an over-defined problem during the interpolation due to the too many points present in one grid cell (Schürch et al., 2011). If we do not consider the systematic error (that will be discussed separately later), the law of large numbers (Kromer et al., 2015) indicates that the accuracy will increase when average is performed, assuming that the surface is locally planar, at the centimetre scale. As an example, considering the lower accuracy is $\sigma_1 = 8$ mm, but the average is performed on a 4 cm^2, (2 cm × 2 cm), with density ranging from 0.3 to 3 pts cm^{-2} ($n = 1.2$ and 12 pts in 4 cm^2) we obtain an accuracy ranging from 6.7 to 2.3 mm, because $\sigma_n = (\sigma_1\, n^{-1})^{0.5}$. In some cases, TLS data can allow detecting movements below 1 mm, because of the law of large number (Kromer et al., 2015).

3.3 Calculation of vertical difference images: location of erosion-prone areas and quantification of volume changes

To quantify and map the ablation and deposition through time, the most recent DEM was subtracted from the earlier (DeRose et al., 1998). The resulting elevation changes have negative pixel values representing ablation and positive pixel values representing deposition.

Eleven difference images have been calculated from the 9 May 2007 to the 4 November 2010 (Fig. 2). Because the occurrence of processes is strongly related to each season, the images are sorted out by seasonal periods. The mapping of the different ablation and deposition areas is carried out for each season by taking into account the difference image of the corresponding season. These comparisons allow the detection and mapping of the most ablation-deposition-prone areas in the catchment (Fig. 3), and the characterization of the annual pattern of erosion (Betts and DeRose, 1999). These maps represent a synthesis of the difference images of Fig. 2, including the interpretation in terms of dominant ablation or deposition process. On these maps

(Fig. 3), the ablation areas are displayed in orange and the deposition areas are in blue (see also the video in the Supplement).

To quantify the volume of soil surface changes, the elevation differences are summed and multiplied by the DEM squared cell resolution ($0.004\,\mathrm{m}^2$). To obtain the sediment budget, the total volume of deposition is subtracted to the total volume of erosion. This calculation provides the final results of topographic changes in cubic meters. To minimize scan alignment inaccuracy on the quantification of the volumes, the topographic changes outside the active erosion–prone areas previously mapped have been ignored. Finally, an average density ($1500\,\mathrm{kg\,m}^{-3}$) of the black marls deposits measured in the sediment trap (Mathys et al., 1996) is used to correct the estimated TLS volumes, because of the vegetated area and the occlusions which are not imaged by the scans. The density of the eroded material changes throughout the year according to the seasons as shown in Table 2.

3.4 Comparisons of the TLS sediment budget to the observed bedload transport

The results have been compared to the bedload transport monitored in the sediment trap, which is measured manually after each significant rainfall. Because annually an average of 20 % of the total eroded sediment exits the catchment in water-suspended flows the budget sediment trap sediment have been increased by 20 %. It must be noted that during major storm events, up to 40 % of sediments can exit the catchment in hyperconcentrated flows (Mathys, 2006).

3.5 Sources of errors

The use of TLS observations resulted in several sources of errors that are quantified. First, TLS measurements are affected by instrumental errors as described by Abellán et al. (2009). Second, some scans are also affected by deformation due atmospheric conditions. Third, some difference images had some misalignment characterized by

slight tiling due to scan deformation and/or scan alignment inaccuracies; such a source of error is for instance clearly visible on Fig. 4f. In fact, the quality precision and precision of the two successive alignment procedures, i.e. the scan merging and the "geo-referencing" vary from a measurement campaign to another as the TLS instrument, the scan deformation and the spatial resolution were different (Table 2).

A possible procedure to estimate the overall errors is to define the quality of the alignments for each campaign (1) and between them (2). This corresponds to the measures of the dispersion of the points between two merged scans (1). This is performed by identifying the areas that have not changed (fixed surfaces like the sphere; wall, etc.) match. The average distance between two scans and the associated standard deviation is performed using the point to surface method. (2) Similar procedure can be applied to successive campaigns. Note that the interpolation of the HRDEM allows reducing the noise and minimizing other measurement errors.

4 Results

4.1 Analysis of soil surface height differences

Difference images outline the slope surface changes at a centimetre scale (Fig. 2). All the images are presented in a plan view on a hillshade of the watershed. The eastern limit of the catchment lacks in data because of a dense vegetation cover. The differences under 1.8 cm are not displayed. This limit has been chosen on a trial and error procedure, and assuming that it contains in most cases above three times the maximum error of alignment of 6 mm, except for the scans of 2007. A clustering of the height differences in three classes is proposed both for the ablation and deposition; small height differences ranging from 1.8 to 4.0 cm, moderate height differences ranging from 4.0 to 10.0 cm, high height differences above 10.0 cm in absolute value. The ablation pattern is displayed in warm colours while the deposition pattern is displayed in cold colours.

4.2   Cartography and temporal pattern of erosion processes

Five erosion patterns are distinguished for La Roubine catchment; winter, spring, late spring–early summer, summer and autumn:

- Winter seasons erosion pattern is illustrated by the elevation difference image between the 3 November 2009 and the 23 March 2010 (Fig. 2g).

- Spring seasons erosion pattern is represented by the elevation difference images between the 14 April to the 1 June 2009 and the 23 March to the 28 May 2010 (respectively Fig. 2d and h);

- The erosion pattern of late spring - early summer rainy season is illustrated by the elevation difference images between the 9 May 2007 to the 24 June 2007 and the 28 May to the 23 June 2010 (respectively Fig. 2a and i). In 2009, the rainfall amount at this season was 30 % below average up to 20 December, and 19 % below average for the whole year, only thanks to some late precipitations in the last days of the calendar year, most probably snow. Thus no difference image corresponds for that period in 2009;

- Summer season erosion pattern is represented by the elevation difference images between the 1 June to the 11 August 2009 and the 23 June to the 22 September 2010 (respectively Fig. 2e and j);

- Autumn season erosion pattern is represented by the elevation difference images between the 11 August to the 3 November 2009 and the 22 September to the 4 November 2010 (respectively Fig. 2f and k).

During winter seasons, (Fig. 3e) the alternating freezing-thawing cycles favour the regolith development. Gelifluction (and solifluction during thawing) in the upper parts of the gullies and on the steep slopes surrounding the gullies lead to an accumulation of material in the lower parts of the gullies. The soil surface changes are mostly located

on the south-facing slopes of the watershed. Higher number of freezing-thawing cycles result in a higher amount of regolith that can be mobilized (Maquaire et al., 2002; Raclot et al., 2005) and therefore more production of sediment along the slopes.

During the spring seasons, (Fig. 3a), the sediment accumulated during winter in the main gullies is transported at the outlet of the catchment. This transport is generally limited to the two main gullies. Ablation is transport-limited and consequently only the gullies with the larger contributing surface are drained. This is probably mainly caused by the limited amount of intense rainfall during that period. Looking at the flow accumulation, the gullies that have a contributive area smaller than $100\,m^2$ are not able to mobilize material if the daily rainfall or the intensity is not sufficient. To give an order of magnitude, if an intense event of a few minutes at $0.5\,mm\,min^{-1}$ occurs on a saturated ground, and assuming 100 % runoff, the discharge will be of $0.5\,L\,min^{-1}$ which probably permits to erode the rills.

During late spring–early summer rainy seasons, (Fig. 3b), the rainfall can be relatively intense (Mathys et al., 2005). Consequently, the secondary rills, gullies and the steepest slopes can be strongly affected by Hortonian runoff and the weathered regolith developed during winter can be washed out. The south-facing slopes are more prone to such type of erosion pattern as more weathered sediment is produced during winters. Very often, small deposition levees are observed at the lower (flatter) parts of the gullies.

During the summer seasons (Fig. 3c), characterized by a relatively dryness except the occurrence of a few thunderstorms, there is very little erosion activity. The same small gullies and rills than those affected by the late spring erosion pattern are continued to be eroded in their steepest parts while deposits and small levees are formed in their lower parts. Most of the loose weathered regolith has already been washed away. The less frequent but more intense storms observed in this season do not impact the erosion pattern, now sediment-limited.

During the autumn seasons (Fig. 3d), the rainfall pattern is characterized by long and low intensity events with some very short intense precipitation prone to a slow soil

wetting and consecutive increase in soil moisture. Progressively, a new layer of regolith is created, and in most of the rills and gullies, sediment transport is reactivated.

4.3 Quantification of seasonal sediment budget changes

For the quantification of the seasonal sediment budget changes, the TLS data of the years 2007 and 2008 have been ignored, because TLS data were not covering the largest possible area of the catchment as other did. The eroded volumes estimated with TLS (Table 2) are in agreement with the integrated measurement of coarse sediment transfer at the outlet trap (Table 3; Fig. 4), the difference is in an acceptable range (5.5 % for the period from 14 April 2009 to 4 November 2010 on the total cumulated volumes).

The maximum eroded volume is produced for the period March–June 2010 (Table 2) with a sediment transfer of ca. $8.7 \, \text{m}^3$ out of the catchment. For the period November 2009–March 2010 (Table 2) more than $4 \, \text{m}^3$ are transported but most of the volume is redistributed within the catchment because the rainfall were not intense enough to transport the sediments out of the catchment. The autumns 2009 and 2010 (Table 2) are characterized by moderate sediment transfers with respectively 0.9 and $1.7 \, \text{m}^3$ transported out of the catchment based on TLS observations, with some significant rainfall events. It must be noted that the event of the 21 October 2009 led to a deposit of $1.7 \, \text{m}^3$ in the sediment trap, with an intensity reaching $0.8 \, \text{mm} \, \text{min}^{-1}$ and rain totalling $36 \, \text{mm}$ during the day. The three main events of 2010 are of different types. The first occurred during the 14 first days of May for a total of precipitation of $155 \, \text{mm}$. The main precipitation event occurred on 10 May which reached $1 \, \text{mm} \, \text{min}^{-1}$ (during four minutes more than $0.5 \, \text{mm} \, \text{min}^{-1}$) after antecedent precipitations since 1 May of $70 \, \text{mm}$. A volume of nearly $3 \, \text{m}^3$ was transferred out of the catchment during that period. The second occurred on the 15 June 2010 with a daily rainfall of $69 \, \text{mm}$, with the day before $5.5 \, \text{mm}$ including an intensity maximum of $0.8 \, \text{mm} \, \text{min}^{-1}$. The maximum intensity of the 15 was of $0.6 \, \text{mm} \, \text{min}^{-1}$ after $42 \, \text{mm}$ of antecedent precipitation (from the 14). It appears that this event was able to transport out of the catchment around $3 \, \text{m}^3$ measured

in the trap and estimated at $6\,\mathrm{m}^3$ from TLS for the period 28 May–23 June 2010. The last important event occurred on 4 October 2010, with a small but intense 12 mm rain event. The intensity reached $1\,\mathrm{mm\,min}^{-1}$ during 10 min. The measurements by TLS ($1.6\,\mathrm{m}^3$) and within the sediment trap ($1.7\,\mathrm{m}^3$) were very close.

5 Interpretation and discussion

The two values of eroded volumes (TLS and sediment trap increased by 20 % to include the suspend sediments) are underestimations of the true erosion rate. With the TLS measurements, the balance value is negative when the ablation sediment volume is larger than the deposited sediment volumes. The presence of shadow areas in the TLS scans affects the TLS sediment budget as erosion-prone areas can be hidden from the laser pulse. When these erosion-prone areas are hidden, the deposited sediments can be estimated as more important than the ablation volumes. The balance is therefore positive, as for example for the period June–September 2010 (Table 2). The shadow areas are usually located in the upper parts of the slopes, often very steep and close to the crests of the catchment; these areas are highly productive source of sediments Therefore, it is hypothesized that the sediment budget is underestimated for most of the periods. In addition, although the swelling or inflation of the regolith surface (Bechet et al., 2015) can have an influence on the georeferencing, it was not possible to quantify it at the level of La Roubine catchment.

Also, topographic height differences smaller than the TLS threshold we used, i.e. 1.8 cm, are not integrated in the sediment budget while they could contribute to an important sediment volume because of their possible widespread occurrence, mainly during the summer storms that trigger important Hortonian runoff. This limitation also influences the sediment budget by underestimating the total volume of ablation. But because of the coherence of the results, we consider that it can be a base for an interpretation of the catchment erosional system.

5.1 Synthesis

All the results can be synthesized in a conceptual model describing the seasonal pattern of ablation and deposition and quantifying the volumes of sediment transfer (Fig. 5). This seasonal pattern is controlled by the rainfall distribution and the availability of sediment during each period. The results may thus be different depending on the year but the sequence will not change, only the time lapses between major erosive events will change.

During the spring and summer seasons, the sediment transfer consists of the ablation of the weathered loose regolith layer on the slopes and a mobilization of the transient storages of accumulated sediments in the rills and gullies, if no exceptional rainfall eve occurs. Most of the sediment exiting the Roubine catchment are a product of the winter weathering. The erosion progressively evolves from a transport-limited (at the beginning of spring) to a supply-limited (in summer) pattern. However, diffuse ablation may happen during intense summer storms as heavy drops may detach small particles and Hortonian runoff may be generated. This process could not be measured with the TLS technique as a higher accuracy is necessary. In the autumn seasons, a new layer of loose regolith is progressively created, and if an intense rainfall event has occurred before in summer as it is usually the case, then the quantity of available sediment is limited.

The main events summarized above all occurred after more than 9 mm rainfall, which is also the limit for initiating runoff in a larger similar catchment (Laval) after more than 5 antecedent dry days (Mathys et al., 2000), that threshold going down with if the dry period goes below 5 days. These events possess either intensity that reaches $1\,\mathrm{mm\,min^{-1}}(= 60\,\mathrm{mm\,h^{-1}})$, which is the limit to trigger MDF's (Yamakoshi et al., 2009) or with immediate antecedent rainfall that has saturated the soil. This last situation permits to initiate earlier the runoff, if it is coupled with significant precipitation, which permits to induce an erosion pulse with lower intensities such as $0.6\,\mathrm{mm\,min^{-1}}$. The sediment yield is controlled by the availability of the upper part of regolith and by the

grain size distribution. Mathys (2006) indicated that in the area of Draix the four first centimetres of the regolith contain 45 % clay and silts and 4–8 cm contains 35 % clays and silts. This shows that the size of material transported will change with time, i.e. antecedent period in terms of rainfall and climate. In addition, it has been shown that in

5 the beginning of the year the sediment moves but stay partially within the catchment, concentrating the material in the gullies. This non-linearity is supported by the fact that the quantity and type of material mobilized depends on the duration and intensity of the rainfall. Partitioning of the total load exported from the catchment shows that at low discharge the suspended material part ranges between 0 and 40 %, whereas it is

10 close to 40 % for higher discharge (Mathys, 2006). This indicates that only high intensity precipitations can mobilize the whole upper part of the regolith and/or split marl plates in smaller particles, whereas small intensities depend on the grain size of this upper part of the regolith at the time of the event.

It is also clear that sediment transfer depends on the material available (Bardou

15 and Jaboyedoff, 2008). The winter period, because of frost/thaw cycles and low rainfall intensity, permits to create and accumulate weathered material. The relatively low rainfall intensities of these winter periods permit to mobilize partially material that remains within the slope and gullies.

The difference between rills and inter-rills erosion depends on rainfall intensity, and

20 antecedent rainfall amounts. The accumulated material in the rills can be mobilized by moderate rainfall intensities for fine material, while inter-rills need intense precipitations and/or a well-developed upper part of the regolith. In winter, the material probably only moves by solifluction of the upper regolith on short distance, i.e. cm to a few meters. In spring, the material accumulated in the rill is washed away, and later the inter-rills

25 and rills with small contributing areas can be eroded and the material transported outside the catchment. Autumn permits to clean the material accumulated during summer in the main rills. This scheme may change depending on the future climate, if less precipitation occurs and only intense rainfall event remains. The system could then concentrate the full erosion in one or a few events. A warmer climate may also reduce

the number of frost-thaw cycles and thus also reduce the depth of the regolith layer generated every year. But in any case the seasonality that leads to weathered material will remain in the cold period, which is the main producer of sediments that can be mobilized.

6   Conclusion

By their strong and rapid responses to climate forcing, the black marls of Draix-Bléone are favourable to the analysis of erosive processes. This article confirmed results of previous works. The strong dependence to the seasons and the cycle of processes (Jacome, 2009) or the sediment trap measurements and the density of the regolith (Mathys, 2006). The prediction of the responses of small mountain watersheds to climatic events is improved. TLS has proved to be an appropriate tool to monitor gully erosion while being easily reproducible and accurate all at once. It also allowed working at the centimeter scale with success. The method used to create and compare DEMs proved very effective to map and quantify topographic changes, but some difficulties have still to solve to fully quantify the sediment transfer.

The TLS permits mainly to locate the different processes. This first results are showing that the rainfall pattern, i.e. time-series, intensity and duration, controls the sediment delivery sequence, but the process of weathering is fundamental to provide material for either suspended load or bed load. The interplay of rainfall and weathering creates the seasonal pattern.

Here we have shown the limits of the methods. Further investigations with HRDEM must be carefully set up in order to avoid the error coming from data acquisition. These surface monitoring must be coupled with more variables monitored during the event simultaneously such as soil moisture, the swelling, rain drop size, the grainsize distribution, the density, etc. Furthermore density map of the regolith of the catchment throughout the year (season by season) would be a great help to improve the TLS volume correction.

Such procedures are not possible in the Roubine catchment, which must not be perturbed by human activity. A new small catchment (Roubinette) has thus been instrumented on the site of Draix, which will permit to install instruments inside the watershed itself. Another next step will be to acquire TLS data during a storm event.

The Supplement related to this article is available online at doi:10.5194/-15-1555-2015-supplement.

References

Abellan, A., Jaboyedoff, M., Oppikofer, T., and Vilaplana, J. M.: Detection of millimetric deformation using a terrestrial laser scanner: experiment and application to a rockfall event, Nat. Hazards Earth Syst. Sci., 9, 365–372, 2009, http://www.nat-hazards-earth-syst-sci.net/9/365/2009/.

Antoine, P., Giraud, A., Meunier, M., and van Asch T. W. J.: Geological and geotechnical properties of the "Terres Noires" in southeastern France: weathering, erosion, solid transport and instability, Eng. Geol., 40, 223–234, 1995.

Ballais, J.-L.: Apparition et évolution du modelé de roubines dans les Préalpes du Sud: l'exemple de Draix, CAGÉP - URA 903 du CNRS, Institut de Géographie de l'Université de Provence, 1999.

Bardou, E. and Jaboyedoff, M.: Debris Flows as a Factor of Hillslope Evolution controlled by a Continuous or a Pulse Process? in: Landscape Evolution: Denudation, Climate and Tectonics over Different Time and Space Scales, edited by: Gallagher, K., Jones, S. J., and Wainwright, J., J. Geol. Soc. London, 296, 63–78, 2008.

Bechet, J., Duc, J., Jaboyedoff, M., Loye, A., and Mathys, N.: Erosion processes in black marl soils at the millimetre scale: preliminary insights from an analogous model, Hydrol. Earth Syst. Sci., 19, 1849–1855, doi:10.5194/hess-19-1849-2015, 2015.

Besl, P. J. and McKay, N. D.: A method for registration of 3-D shapes, IEEE T. Pattern. Anal., 14, 239–256, 1992.

Betts, H. D. and DeRose, R. C.: Digital elevation models as a tool for monitoring and measuring gully erosion, JAG, 1, 91–100, 1999.

Brochot, S. and Meunier, M.: Erosion de badlands dans les Alpes du Sud – Synthèse, CEMA-GREF division protection contre les érosions, mars 1994, Grenoble, France, 1994.

Chen, Y. and Medioni, G.: Object modeling by registration of multiple range images, Image Vision Comput., 10, 145–155, 1992.

DeRose, R. C., Gomez, B., Marden, M., and Trustrum, N. A.: Gully erosion in Mangatu Forest, New Zealand, estimated from digital elevation Models, Earth Surf. Proc. Land., 23, 1045–1053, 1998.

Descroix, L. and Olivry, J. C.: Spatial and temporal factors of erosion by water of black marl in the badlands of the French Southern Alps, Hydrolog. Sci. J., 47, 227–242, 2002.

Descroix, L. and Gautier, E.: Water erosion in the southern French Alps: climatic and human mechanisms, Catena, 50, 53–85, 2002.

Descroix, L. and Mathys, N.: Processes, spatio-temporal factors and measurements of current erosion in the French southern Alps: a review, Earth Surf. Proc. Land., 28, 993–1011, 2003.

Innovmetric Software Inc.: Polyworks, version 9.1.8., http://www.innovmetric.com, 2010.

Jaboyedoff, M., Oppikofer, T., Abellán, A., Derron, M.-H., Loye, A., Metzger, R., and Pedrazzini, A.: Use of LIDAR in landslide investigations: a review, Nat. Hazards, 61, 5–28, doi:10.1007/s11069-010-9634-2, 2012.

Jacome, A.: MNT à très haute résolution spatiale pour la représentation 3D des ravines d'érosion de montagne, Thèse de Doctorat, Université Montpellier II, Sciences et Techniques du Languedoc, 2009.

Kromer R, Abellán A., Hutchinson, J., Lato, M., Edwards, T., and Jaboyedoff, M.: A 4D filtering and calibration technique for small-scale point cloud change detection with a Terrestrial Laser Scanner, Remote Sens., 7, 13029–13052, doi:10.3390/rs71013029, 2015.

Légier, A.: Mouvement de terrain et e'volution re'cente du relief dans la re'gion de Barcelonnette (Alpes-de-Haute-Provence), PhD Thesis, Grenoble I University, 163 pp., 1977.

Detection of seasonal erosion processes at the scale of an elementary black marl gully

J. Bechet et al.

Lopez Saez, J., Corona, C., Stoffel, M., Rovéra G., Astrade, L., and Berger, F.: Mapping of erosion rates in marly badlands based on a coupling of anatomical changes in exposed roots with slope maps derived from LiDAR data, Earth Surf. Proc. Land., 36, 1162–1171, doi:10.1002/esp.2141, 2011.

5 Malet, J. P., Auzet, A. V., Maquaire, O., Ambroise, B., Descroix, L., Esteves, M., Vandervaere, J. P., and Truchet, E.: Investigating the influence of soil surface features on infiltration on marly hillslopes. Application to callovo-oxfordian black marls slopes in the Barcelonnette basin (Alpes-de-Haute-Provence, France), Earth Surf. Proc. Land., 28, 547–564, 2003.

Maquaire, O, Ritzenthaler, A., Fabre, D., Thiery, Y., Truchet, E., Malet J- P., and Monnet, J.:
10 Caractérisation des profils de formations superficielles par pénétrométrie dynamique à énergie variable: application aux marnes noires de Draix (Alpes-de-Haute-Provence, France), C. R. Geosci., 334, 835–841, 2002.

Maquaire, O., Malet, J.-P., Remaître A., Locat, J., Klotz, S., Guillon, J.: Instability conditions of marly hillslopes: towards landsliding or gullying? The case of the Barcelonnette Basin, South
15 East France, Eng. Geol., 70, 109–130, 2003.

Mathys, N.: Analyse et modélisation à différentes échelles de mécanismes d'érosion et de transport de matériaux solides. Cas des petits bassins versants de montagne sur marne (Draix, Alpes-de-Hautes-Provence), PhD Thesis, Institut National Polytechnique de Grenoble, 2006.

20 Mathys, N., Brochot, S., and Meunier, M.: L'érosion des terres noires dans les Alpes du Sud: contribution à l'estimation des valeurs annuelles moyennes (bassins versants expérimentaux de Draix, Alpes-de-Haute-Provence, France), CEMAGREF, Grenoble, 1996.

Mathys, N., Brochot, S., and Lacheny, B.: Genèse des crues et érosion dans les petits bassins versant de montagne: observations et résultats obtenus sur les bassins versants expérimen-
25 taux de Draix (Alpes-de-Haute-Provence), Association Forêt Méditerranéenne, XXI, 182–190, 2000.

Mathys, N., Brochot, S., Meunier, M., and Richard, D.: Erosion quantification in the small marly experimental catchment of Draix (Alpes-de-Haute Haute-Provence, France). Calibration of the ETC rainfall–runoff-erosion model, Catena, 50, 527–548, 2003.

30 Mathys, N., Klotz, S., Esteves, M., Descroix, L., and Lapetite, J.-M.: Runoff and erosion in the Black Marls of the French Alps: observations and measurements at the plot scale, Catena, 63, 261–281, 2005.

Title Page

Abstract | Introduction

Conclusions | References

Tables | Figures

|◄ | ►|

◄ | ►

Back | Close

Full Screen / Esc

Printer-friendly Version

Interactive Discussion

Meunier, M. and Mathys, N.: Panorama synthétiques des mesures d'érosion effectuées sur trois bassins du site expérimental de Draix (Alpes-de-Haute Haute-Provence, France), CEMA-GREF, Grenoble, 1995.

Olivier, J. E.: Les fortes crues d'août 1997 à Draix: d'un printemps sec à des records de charges solides, Les bassins versants expérimentaux de Draix laboratoire d'étude de l'érosion en montagne - actes du séminaire, Draix Le Brusquet Digne, 22–24 octobre 1997, Cemagref Editions, Antony, 53–63, 1999.

Olivry, J.-C., and Hoorelbeck, J.: Erodibilité des terres noires de la vallée du Buëch (France, Alpes du Sud), Cahiers ORSTOM.Série Pédologie, 25, 95–110, 1989.

Oostwoud Wijdenes, D. J. and Erzinger, P.: Erosion and sediment transport on steep marly hillslopes, Draix, Haute-Provence, France: an early experimental field study, Catena, 33, 179–200, 1998.

Perroy, R. L., Bookhagen, B., Asner, G. P., and Chadwick, O. A.: Comparison of gully erosion estimates using airborne and ground-based LiDAR on Santa Cruz Island, California, Geomorphology, 118, 288–300, 2010.

Phan, T. S. H. and Antoine, A.: Mineralogical and geotechnical characterization of the "Black Lands" of the South-East of France, having in view road applications, in: Proceedings of the VIIth International Congress of the Intenational Association of Engineering Geology, Lisboa, 5–9 September 1994, vol. 2., Balkema, Rotterdam, 961–966 pp., 1994.

Poesen, J., Nachtergaele, J., Verstraeten, G., and Valentin, C.: Gully erosion and environmental change: importance and research needs, Catena, 50, 91–133, 2003.

Puech, C., Thommeret, N., Kaiser, B., Bailly, J.-S., Jacome, A., Rey, F., and Mathys, N.: MNT à très haute résolution dans les modelés fortement disséqués: des données aux tests d'application, Géomorphologie, 2, 141–152, doi:10.4000/geomorphologie.7589 , 2009.

Raclot, D., Puech, C., Mathys, N., Roux, B., Jacome, A., Asseline, J., and Bailly, J.-S.: Photographies aériennes prises par drone et modèle numérique de terrain: apports pour l'observatoire sur l'érosion, Géomorphologie, 1, 7–20, doi:10.4000/geomorphologie.209, 2005.

Richard, D.: les Les bassins versants experimentaux expérimentaux de Draix (04): éetude de l'érosion et du transport solide torrentielle à partir de mesures in situ, CEMAGREF, Grenoble, 218–228, 1997.

Rovera, G. and Robert, Y.: Conditions climatiques hivernales et processus d'érosion périglaciaires dans les badlands marneux de Draix, Geogr. Phys. Quatern., 59, 31–48, 2005.

Title Page

Abstract | Introduction

Conclusions | References

Tables | Figures

◄ | ►

◄ | ►

Back | Close

Full Screen / Esc

Printer-friendly Version

Interactive Discussion

Schürch, P., Densmore, A. L., Rosser, N. J., Lim, M., and McArdell, B. W.: Detection of surface change in complex topography using terrestrial laser scanning: application to the Illgraben debris-flow channel, Earth Surf. Proc. Land., 36, 1847–1859, 2011.

Shan, J. and Toth, K.: Topographic Laser Ranging and Scanning: Principles and Processing, CRC Press, Taylor & Francis Group, LLC, UK, 2008.

Shepard, D.: A two-dimensional interpolation function for irregularly spaced data, in: Proceedings of 23rd ACM National Conference, New York, 27–29 August 1968, 517–523, doi:10.1145/800186.810616, 1968.

Travelletti, J., Sailhac, P., Malet, J.-P., Grandjean, G., and Ponton, J.: Hydrological response of weathered clay-shale slopes: water infiltration monitoring with time-lapse electrical resistivity tomography, Hydrol. Process., 26, 2106–2119, doi:10.1002/hyp.7983 2012.

Valentin, C., Poesen, J., and Yong, L.: Gully erosion: impacts, factors and control, Catena, 63, 132–153, 2005.

Yamakoshi, T., Mathys, N., and Klotz, S.: Time-lapse video observation of erosion processes on the black marls badlands in the Southern Alps, France, Earth Surf. Proc. Land., 34, 314–318, 2009.

Yamakoshi, T., Mathys, N., and Klotz, S.: Visual observation of erosion processes on the Black Marl badlands in the southern Alps, France, in: Weathering as a Predisposing Factor to Slope Movements, edited by: Calcaterra, D. and Parise, M., Geological Society, London, 23, 201–212, 2010.

Detection of seasonal erosion processes at the scale of an elementary black marl gully

J. Bechet et al.

Title Page

Abstract | Introduction

Conclusions | References

Tables | Figures

Back | Close

Full Screen / Esc

Printer-friendly Version

Interactive Discussion

Table 1. Characteristics of the TLS alignment with, for each time period, with the information on the number of scans used to create a scene. The table indicates standard deviation of the point to the surface matched (point to surface ICP), the mean difference between two scans (either used for to align on period or for inter period comparison), the used average point density and the standard deviation of the average mean difference.

Period of time	Num. scans	SD Pts. -Surf. [m]	Mean diff. align. [m]	Pts. Density [pts cm^{-2}]	SD mean diff. [m]	SD inter period [m]	Mean diff. Inter period [m]	Pts. density [pts cm^{-2}]	SD mean diff. [m]
		Alignment scans of each period				Inter-period			
May 2007 (O)	3	0.0060	0.000010	1.257	2.0895E-06	0.01500	−0.00027	72.431	3.4037E-05
Jun 2007 (O)	1	–	–	0.776	–	0.01328	−0.00006	4.975	1.0768E-05
Jun 2008 (O)	3	0.0070	0.000020	1.374	2.2674E-06	0.00694	−0.00017	2.621	4.3454E-06
Apr 2009 (O)	6	0.0120	0.000034	1.487	3.0478E-06	0.00547	−0.00011	–	–
Jun 2009 (O)	4	0.0046	0.000070	1.315	1.2685E-06	–	–	–	–
Aug 2009 (O)	7	0.0052	0.000008	1.585	1.3217E-06	0.00556	−0.00013	–	–
Nov 2009 (L)	4	0.0042	0.000020	0.610	1.8677E-06	0.00520	0.00028	–	–
Mar 2010 (L)	3	0.0034	0.000043	0.348	2.0170E-06	0.00385	0.00038	–	–
May 2010 (O)	6	0.0046	0.000009	3.094	7.6515E-07	0.00517	−0.00008	8.693	3.2734E-06
Jun 2010 (O)	6	0.0048	0.000007	3.255	7.8926E-07	0.00546	−0.00022	9.991	1.5214E-06
Sep 2010 (L)	3	0.0026	−0.000002	0.179	1.5709E-06	0.00544	0.00929	–	–
Nov 2010 (L)	3	0.0027	0.000030	0.409	1.5128E-06	0.00455	−0.00035	–	–

O = LiDAR Optech Ilris 3-D L = LiDAR Leica TotalStation II.

Table 2. Measured volume of ablation and deposition. In order to perform comparison with Table 3, 0.48 m^3 have been added to the first period to the cumulative volume.

Date start	Date end	Erosion [m^3]	Deposit [m^3]	Balance [m^3]	Cum.Vol. [m^3]
14 Apr 2009	31 May 2009	−0.560	0.265	−0.295	0.8
31 May 2009	11 Aug 2009	−0.382	0.376	−0.006	0.8
11 Aug 2009	3 Nov 2009	−1.992	1.051	−0.941	1.7
3 Nov 2009	23 Mar 2010	−4.537	3.342	−1.195	2.9
23 Mar 2010	28 May 2010	−2.743	0.021	−2.722	5.6
28 May 2010	23 Jun 2010	−6.290	0.256	−6.034	11.7
23 Jun 2010	22 Sep 2010	−0.419	0.053	−0.366	12.0
22 Sep 2010	4 Nov 2010	−1.778	0.160	−1.618	13.7
		Volume added for the 14 Apr 2009			0.48

Table 3. Measured volume in the sediment trap.

Date	Measured volumes [m^3]	Cumulative volumes [m^3]	Date	Measured volumes [m^3]	Cumulative volumes [m^3]
26 Jan 2009	–	–	13 Feb 2010	1.42	5.6
9 Feb 2009	0.48	0.5	5 May 2010	0.01	5.6
17 Apr 2009	0.67	1.2	7 May 2010	0.01	5.6
5 May 2009	0.02	1.2	11 May 2010	2.87	8.5
2 Jul 2009	0.20	1.4	17 May 2010	0.01	8.5
10 Aug 2009	0.09	1.5	16 Jun 2010	3.31	11.8
20 Aug 2009	0.02	1.5	24 Aug 2010	0.49	12.3
27 Sep 2009	0.03	1.5	13 Sep 2010	0.08	12.4
28 Sep 2009	0.24	1.7	22 Sep 2010	0.02	12.4
22 Oct 2009	1.72	3.5	27 Sep 2010	0.32	12.7
4 Nov 2009	0.61	4.1	5 Oct 2010	1.74	14.5
6 Dec 2009	0.12	4.2	25 Oct 2010	0.01	14.5

Detection of seasonal erosion processes at the scale of an elementary black marl gully

J. Bechet et al.
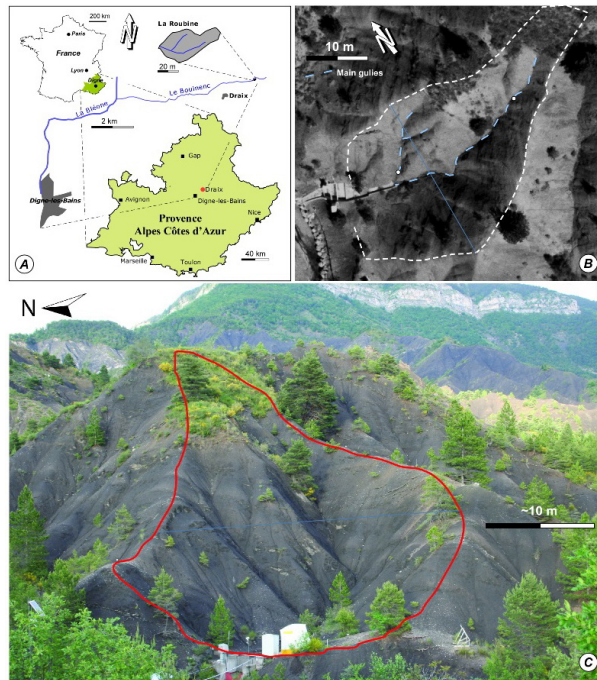
Figure 1. Location and picture of la Roubine. **(a)** Location of la Roubine catchment; **(b)** aerial image of La Roubine. **(c)** Photograph of the Roubine catchment (1 June 2011) with the contours indicated in red line. Foreground: la Roubine catchment characterized by a typical badland morphology, many small scale rills and gullies, steep slopes and scarce vegetation. The catchment outlet is located at the western extremity with the sediment trap and the limnigraph. Background: surrounding badlands and limestone ridge.
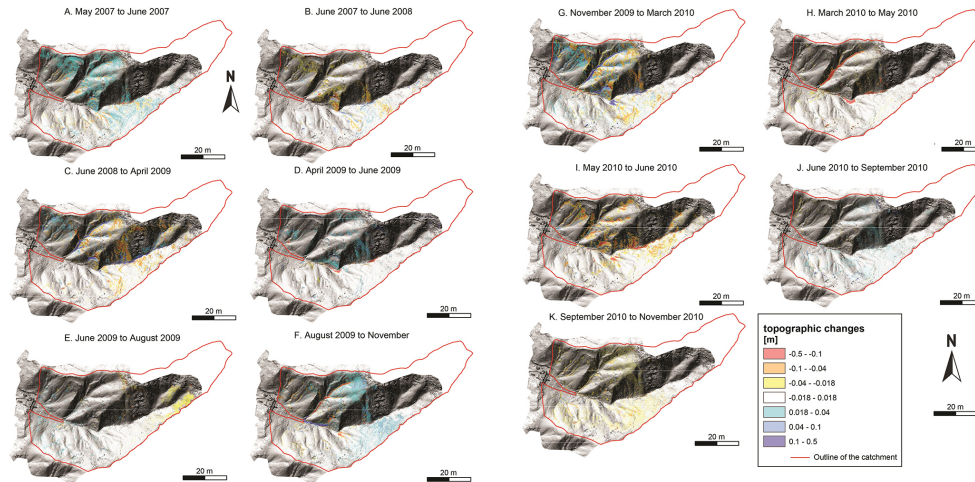
Figure 2. Observed height differences for the period 2007–2010 highlighting the soil surface changes of La Roubine catchment. The red outline indicates the boundary of the catchment.
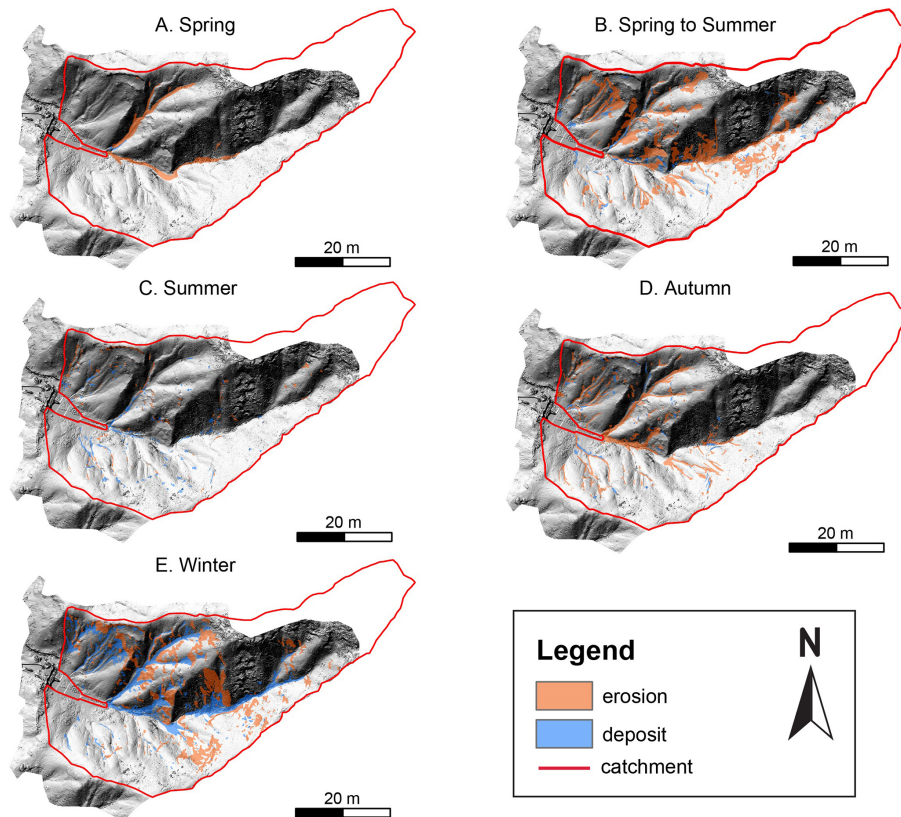
Figure 3. Typical pattern of slope activity (e.g. ablation in orange, deposition in blue) for each predefined seasons. The red outline indicates the boundary of the catchment (see also the video in the Supplement).
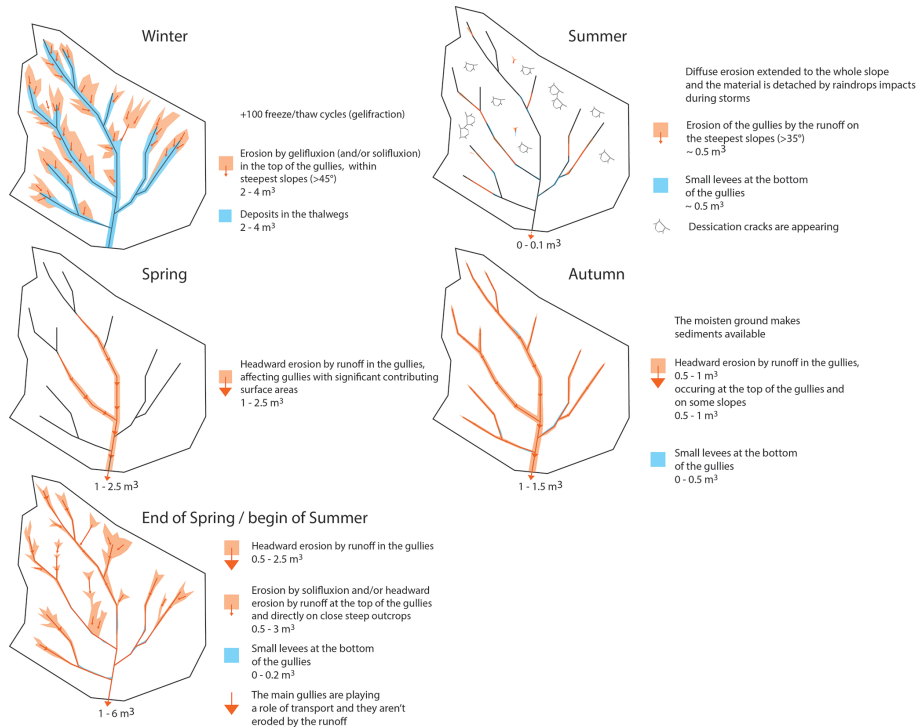
Figure 4. Cumulated TLS measured volumes (in bold black line) against cumulated sediment trap measured volumes (thin black line) for the years 2009 and 2010. In addition, the cumulative precipitation are shown as well as the main daily precipitations events and the largest intensity event.

Figure 5. Conceptual model describing the seasonal pattern of ablation and deposition and quantification of the volumes of sediment transfer at La Roubine catchment.